The local climate impact of photovoltaic solar farms ——Results from a field observation campaign in gobi desert

Xiaoqing Gao, Liwei Yang, Xuhong Hou and Xiaoying Hui

Key Laboratory of Land Surface Process and Climate Change in Cold and Arid Regions, Northwest Institute of Eco-Environment and Resources, CAS, Lanzhou, Gansu (China)

Abstract

Large-scale solar power farms are rapidly increasing in size and number across the world. However, the surface heat balance is altered when a photovoltaic (PV) power plant is deployed. Modifications to the surface albedo through the deployment of photovoltaic arrays have the potential to change radiative forcing, surface temperatures and local weather patterns. In this work, the field observation data from a large solar farm and a region without PV array in Golmud are used to study the impact of large solar farms in desert areas on the local climate. The results show the mean daily albedo in the solar farm is 0.19, while it is 0.26 in the region without PV. The annual mean net radiation in the solar farm is evidently higher than that of the region without PV. The annual range of soil temperatures at depths of 5–180 cm in the solar farm is bigger than that in the region without PV. The soil temperatures at different depths in winter in the solar farm are clearly lower than those in the region without PV. The 2-m daytime air temperature in the two sites is essentially the same during winter, while during the other seasons, the daytime air temperature in the PV farm is higher than that in the region without PV, with the maximum difference appearing in summer. The nighttime air temperatures at the height of 2 m during the four seasons in the solar farm are higher than those in the region without PV.

Keywords: meteorological observation, photovoltaic farm, desert areas, local climatic effect

1. Introduction

Renewable energy is considered an important solution for mitigating global warming, energy crisis and environmental pollution. The predominant renewable energy sources include wind, solar, biomass, hydropower and geothermal. Photovoltaic solar power systems have drawn tremendous attention from government sectors, researchers and the industry over the past several decades (Gagnon et al., 2002; Liu et al., 2015).

Large-scale solar power plants are rapidly increasing in size and number in China, as well as in other parts of the world. Photovoltaic (PV) power plants in desert regions have a promising future in China, considering the intense radiation received in large areas in China. However, the surface heat balance is altered when a photovoltaic power plant is operating. Modifications to the surface albedo through the deployment of photovoltaic arrays have the potential to change radiative forcing, surface temperatures and local weather patterns. Nemet (2009) investigated the net radiative forcing from the widespread installation of photovoltaics on the earth's surface. However, Nemet did not consider local microclimates, nor have his analytical results been verified with any field data. Genchi et al. (2002) estimated the impact of large-scale installation of PV systems in Tokyo on the urban heat island effect. The simulation results showed that it would be negligible. Tian et al. (2007) analyzed the effect of the PV module on the microclimate of the urban canopy layer, with the simulation results showing that the urban canopy air temperature alters little and the increase in the PV conversion efficiency can reduce the urban canopy air temperature. Taha (2013) evaluated the potential atmospheric effects of PV deployment in urban areas and the simulation results showed a 1–2 ℃ decrease in peak urban temperatures at six locations across California. Turney and Fthenakis (2011) identified 32 categories of impacts from the installation and operation of large-scale solar power plants. They found the impacts were either beneficial or neutral, except the local climate effect, for which they concluded that research and observations were needed.

The potential effects of the deployment of PV panels on climate have been discussed in previous studies. However, most of these studies focus on urban areas and use simulation methods. In this work, the impact of solar farms on the local meteorology in desert areas is assessed with observational data. It is believed that the results from this research can provide basic data support for the simulation of the local climate effect of a photovoltaic power station.

doi:10.18086/swc.2017.22.01 Available at http://proceedings.ises.org

Moreover, it may be useful for guiding the development and appropriate utilization of solar energy.

2. Materials and methods

2.1. Study area and field experiment description

The observation data is taken from Golmud (36°21′55″N; 95°06′48″E; a.s. 2868 m), Qinghai Province. After Tibet, the solar radiation in Golmud is the highest in China. Located at the south edge of the Qaidam Basin, the solar farm covers an area of 2.37 square kilometers, measuring 2296 meters from east to west and 1271 meters from north to south. The type of landform is Gobi Desert, with a continental plateau climate. The dominant wind direction in Golmud is the westerly wind.

Photovoltaic arrays are fixed. The azimuth of a PV array is south, with a tilt angle of 36°, a height of 2.5 m, and a spacing between each PV row in the solar farm of 6 m. The solar conversion efficiency of the solar panels is 15%. There are two observation points in this test; one is in the photovoltaic power station (site A), located at 36°20.128' N, 95°13.372' E at an altitude of 2927 m. The underlying surface is the Gobi. Detailed measurements taken at a height of 10 m were wind speed, wind direction, air temperature, humidity and solar radiation, while measurements taken at a height of 2 m were wind speed, wind direction, air temperature and humidity. The measurement taken at a height of 1.5 m was solar radiation. Soil temperatures at 5, 10, 20, 40, 80, and 180 cm were recorded in the solar farm. The other measurement point was outside the photovoltaic power station (site B), to be used as a reference point indicating ambient conditions. It was to the southwest of site A, located at 36°19.975' N and 95°12.985' E, at an altitude of 2933 m, with the underlying surface being Gobi with sparse vegetation. Detailed measurements taken at a height of 3 m were wind speed and wind direction, while measurements taken at a height of 2 m were air temperature and humidity. The measurement taken at a height of 1.5 m was solar radiation. Soil temperatures at 5, 10, 20, 40, 80, and 180 cm were recorded in the region without a PV array. The two observation sites were 645 meters apart. The characteristics of the sensors can be found in Table 1. Figure 1 shows an illustration of the solar farm and the locations where the field measurements were taken.

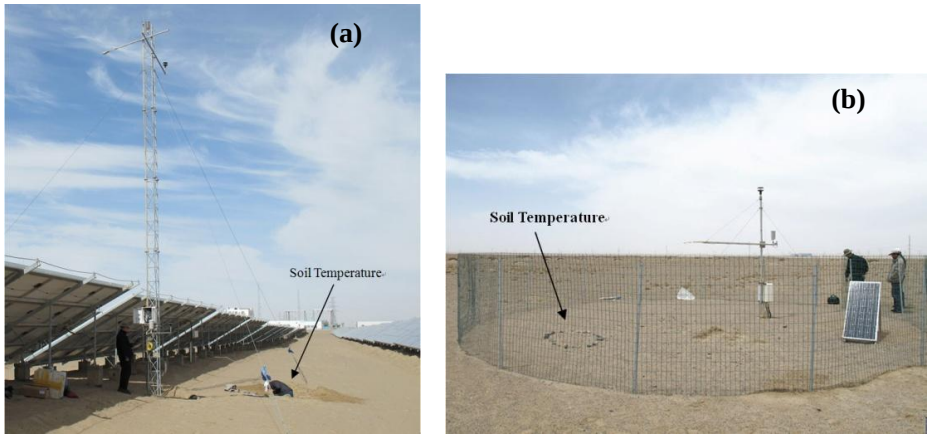

Fig. 1: The illustrations of the two sites in Golmud: (a) in the solar farm (Site A) and (b) in the region without PV (Site B).

2.2. Data and methods

The present work is based on data acquired at a 10-min step since October 2012. All the data have been passed through data quality control. All of the observation times are recorded in Beijing time. NR is deduced from the energy budget equation:

$$NR = (DSR - USR) + (DLR - ULR) \quad \text{(eq. 1)}$$

$$A = USR / DSR \quad \text{(eq. 2)}$$

where NR, DSR, USR, DLR and ULR are net radiation, downward and upward shortwave radiation and downward and upward long wave radiation (W/m^2), respectively. A is albedo (Tyagi et al., 2012). The energy balance equation is:

$$NR = H + LE + G + S_e \quad \text{(eq. 3)}$$

where H is the sensible heat flux, LE is the latent heat flux, G is the soil heat flux, S_e is the

solar panel electricity (Fig. 2). Due to the minimal precipitation in the Gobi area, the latent heat exchange is negligible. The land surface temperature (ST) is related to the surface long wave radiation by the Stefan-Boltzmann law (Wang and Liang, 2009):

$$ULR = \varepsilon_s \cdot \sigma \cdot ST^4 + (1-\varepsilon_s) \cdot DLR \qquad \text{(eq. 4)}$$

where ε_s is the broadband emissivity over the entire infrared region and σ is the Stefan-Boltzmann's constant (5.67×10^{-8} W $\cdot$m^{-2} $\cdot$K^{-4}). In the PV farm, 80% of the underlying surface is the ground, due to which, the emissivity ε_s is approximately 0.95. Therefore, ST can be estimated from Eq. (4). Soil thermal conductivity is calculated by the Harmonic method (Gao et al., 2009) as shown below.

The heat conduction equation (Horton et al., 1983) is:

$$\frac{\partial T}{\partial t} = k\frac{\partial^2 T}{\partial z^2} \qquad \text{(eq. 5)}$$

where T is the soil temperature (℃), t is the time (s), z is the depth (m), k is the thermal diffusivity, $k = \lambda / C_p$, λ is the thermal conductivity (W m^{-1} ·℃$^{-1}$), and C_p is the volumetric heat capacity. The C_p and λ are assumed to be independent of depth and time.

For the Eq. (5), it can be solved without initial conditions in semi-infinite space, and its upper boundary condition is assumed as Fourier series:

$$T(0,t) = \overline{T}(0) + \sum_{i=1}^{n} A_i \sin(i\omega t + \Phi_i) \qquad \text{(eq. 6)}$$

The solution to Eq. (5) using superposition is:

$$T(z,t) = \overline{T}(z) + \sum_{i=1}^{n} A_i \exp(-B_i z) \times \sin(i\omega t + \Phi_i - B_i z) \qquad \text{(eq. 7)}$$

where $\overline{T}$ is the mean soil surface temperature, A is the amplitude of the diurnal soil surface temperature wave, Φ is the phase, n is the number of harmonics, $B_i = \sqrt{i\omega/(2k)}$ is the damping depth of the diurnal temperature wave. If the soil temperature at a depth of z_1 is the upper boundary, the formula for calculating the temperature of soil at any depth by the method of harmonic is:

$$T(z,t) = \overline{T}(z) + \sum_{i=1}^{n} A_i \exp(-B_i(z-z_1) \times \sin(i\omega t + \phi_i - B_i(z-z_1)) \qquad \text{(eq. 8)}$$

In the concrete calculation, the observed data of the two layers of soil temperature can be used to calculate the optimal estimation of the parameters (A_i , Φ_i) in Eq. (6), as well as the parameter (B) in Eq. (8) by using the least square method, thus obtaining the estimated value of soil thermal diffusivity (Horton et al., 1983). Taking the 5-cm soil temperature as the upper boundary (Eq. (6)), the least square method is used to fit different harmonic order numbers, with the second-order harmonic model having a high precision (correlation coefficient r = 0.998). Considering the simplification and precision of the model, the second-order harmonic model (n=2) is used as the model of the harmonic method, C_p =1.47×10^6 J m^{-3} K^{-1}, in this paper. Therefore, soil thermal conductivity can be estimated using Eq. (8).

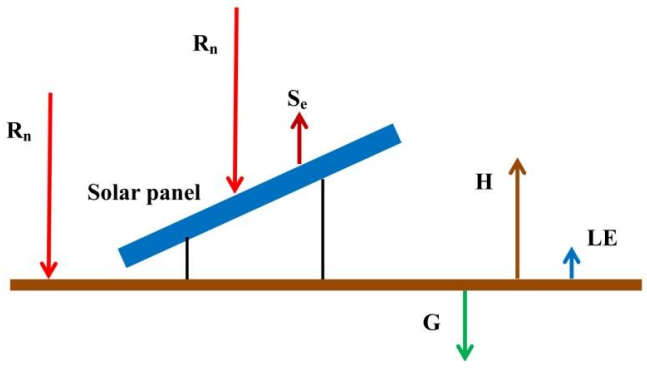

Fig. 2: The conceptual model of the heat balance near the surface in the solar farm

Tab.1: Summary of the instrumentations of sites A and B for the measurement presented in this paper.

Parameter (unit)	Sensor	Height above ground level	Accuracy	Sampling rate (min)	Averaging interval (min)
Air temperature (℃)	Vaisala HMP155A	2, 10 m in Site A; 2 m in Site B	±0.12°C (20℃)	1	10
Relative humidity (%)	Vaisala HMP155A	2, 10 m in Site A; 2 m in Site B	±1% (0~90% RH)	1	10
Short wave radiation incoming and outgoing (W m^{-2})	Kipp and Zonen CNR 4 0.31 < λ < 2.8 μm	1.5, 10 m in Site A; 2 m in Site B	<1% (0~1000 W/m^2)	1	10
Long wave radiation incoming and outgoing (W m^{-2})	Kipp and Zonen CNR 4 4.5 < λ < 42 μm	1.5, 10 m in Site A; 2 m in Site B	<1% (-250~250 W/m^2)	1	10
Soil temperature (℃)	Campbell 109SS-L	-5, -10, -20, -40, -80, -180 cm in Site A and B	±0.2℃ (0~70℃), ± 0.5℃ (-50℃)	1	10
Wind speed (m s^{-1})	Gill WINDSONIC	2, 10 m in Site A; 3 m in Site B	±2%	1	10
Wind direction (°)	Gill WINDSONIC	2, 10 m in Site A; 3 m in Site B	±3°	1	10

3. Results and discussion

3.1. Comparison of the radiation field in the two sites

The surface radiation budget plays an important role in regional climate (Li et al., 2009). The intensity of incoming and outgoing radiative fluxes at the surface in the PV farm depends on the angle of inclination of the PV arrays and their exposure relative to the direction of the incoming solar beam, as well as on the PV system efficiency and the characteristics of the surrounding terrain (Matzinger et al., 2002; Kämpf et al., 2010; Zhang et al., 2016).

The observational data used in this study are from October 2012 to September 2013. The observations at a height of 10 m in the solar farm are 7.5 m higher than the perpendicular height of the PV array. The angle of the upward radiation sensor is 150°, with the field of view of the radiation sensor being the mixed underlying surface area with a 56-m diameter, due to which the radiation data at a height of 10 m is used to discuss the influence of PV array on the radiation field. Figure 3 shows the annual averaged diurnal variations of each component of the radiation budget and surface temperature at the two sites. Figure 4 shows the annual variation in radiation flux at the two sites, each black dot represents 10-min averaged value and Fig. 5 shows the annual variation in the monthly averaged albedo at the two sites.

There is no difference in the downward shortwave radiation (DSR) and the downward longwave radiation (DLR) between the two sites. Therefore, they are not analyzed.

The upward shortwave radiation (USR) reached a peak of approximately 128.8 W m^{-2} at 14:00 in the annual averaged diurnal variations at site A, and 193.7 W m^{-2} at 14:00 at site B, as shown in Fig. 3(a). The daily cumulative value of the USR at site A is 3.54 MJ m^{-2}, while it is 5.02 MJ m^{-2} at site B. The value in the solar farm is 1.48 MJ m^{-2} lower than that in the region without PV, with the difference between the two sites being large. Due to the snow cover during November and December, the surface albedo is higher, which makes the USR on sunny days abnormally high (Fig. 4(a) and (a1)). The monthly averaged USR reached a maximum in June and a minimum in December at site A, while it reached a maximum in April and a minimum in January at site B (Fig. 4(a) and (a1)). The solar conversion efficiency of the solar panels is related to meteorological factors, mainly ambient temperature, dust, wind speed and relative humidity. This causes the peaks and valleys of USR to appear during different months for the two sites. The difference in the values of USR between the two sites is negative during the year, which is evident in Fig. 4(d). The ratio of the average annual USR at site A to that at site B is 0.7 (Table 2), indicating that the response of the PV array to the radiation fields is mainly to enhance the absorption of the downward shortwave radiation, leading to a significant reduction in the upward short wave radiation, with an influence of up to 30%. The difference in the USR at the two sites reached the maximum in March–April (spring), with a value of -20.7 W m^{-2}, while it reached the minimum in December–January of the following year (winter), with a value of -11.6 W m^{-2} (Fig. 4(d)).

The upward longwave radiation (ULR) depends on the surface temperature raised to the power of four (Eq. (4)).

The ULR has diurnal variation with the surface temperature (Li et al., 2009). The ULR reached a peak of approximately 443.0 W m^{-2} at 15:00 at site A, and 471.5 W m^{-2} at 15:00 at site B in Fig. 3(b). The ULR at site A is clearly lower than that at site B during 11:00–18:00, while it is higher during 00:00–9:00, which is mainly due to the change in surface temperature, as shown in Fig. 3(e). The daily cumulative value of the ULR at site A is lower than that at site B, while the cumulative value of the ULR in the daytime at site A is lower than that at site B. The difference is 0.62 MJ m^{-2}. The cumulative value of the ULR at night is 0.12 MJ m^{-2} higher than that at site B, since the PV plants have an insulating effect at night and a cooling effect during daytime. The cooling effect is more noticeable. The monthly average ULR reached a maximum in July and a minimum in January at the two sites, as shown in Fig. 4(b) and (b1). The difference in the values of the ULR between the two sites is negative over a period of one year. The difference in the ULR at the two sites reached the maximum in October, with a value of -8 W m^{-2}. The average annual ULR changed slightly, compared to that at site B. The impact of the PV array on the ULR is no more than 2% (see table 2).

The net radiation (NR) is a measure of the incoming radiation incident on the earth's surface, minus the outgoing energy radiated by the Earth itself. It is related to the four radiation components (Pessacg et al., 2013). The NR reached a peak of approximately 438.0 W m^{-2} at 14:00 at site A, and 366.8 W m^{-2} at 14:00 at site B, as shown in Fig. 3(c). The daily cumulative value of the NR at site A is 8.30 MJ m^{-2}, and 6.34 MJ m^{-2} at site B. The cumulative value of the NR during the daytime at site A is 1.98 MJ m^{-2} higher than that at site B and 0.02 MJ m^{-2} little lower at night. Therefore, the impact of a photovoltaic array on net radiation is mainly during the daytime, which is the photovoltaic power station's main working time. The monthly averaged NR reached a maximum in June and a minimum in December in the two sites, as shown in Fig. 4(c) and (c1). The difference in the values of the NR between the two sites is positive over the entire year, with the difference being evident. The ratio of the average annual NR at site A to that at site B is 1.32, which indicates that the solar farm has been collecting energy. The difference of the NR at the two sites reached the maximum in August, with a value of 33.0 W m^{-2}, while it reached the minimum in December, with a value of 13.2 W m^{-2}.

Surface albedo is the most important parameter affecting the surface radiation budget. As seen from Fig. 3(d), the distribution of the albedos from the two sites are U-shaped, being higher in the morning and evening and lower at noon. When the solar elevation is low, the surface albedo varies greatly. However, with the increase in the solar elevation, the surface albedo decreases and tends to be stable. A large number of photovoltaic devices in the solar farm have a greater capacity to absorb the solar radiation, resulting in lower albedo. The daily average values of surface albedo in the PV farm and without the PV panel are 0.19 and 0.26, respectively. As shown in Fig. 5, the albedos change significantly with the seasons, being lower in summer and higher in autumn and winter. Each seasonal average of the surface albedo at site A is higher than that at site B. The monthly average albedo reached a maximum in November and a minimum in September in the PV area, while it reached a maximum in November and a minimum in July in the region without PV. The difference between the two sites was larger in November 2012 and March 2013, when the average value was 0.11, while it was smaller in May–July, when the average value was 0.05. The annual average values of albedo in the PV farm and the area without the PV panel are 0.19 and 0.27, respectively.

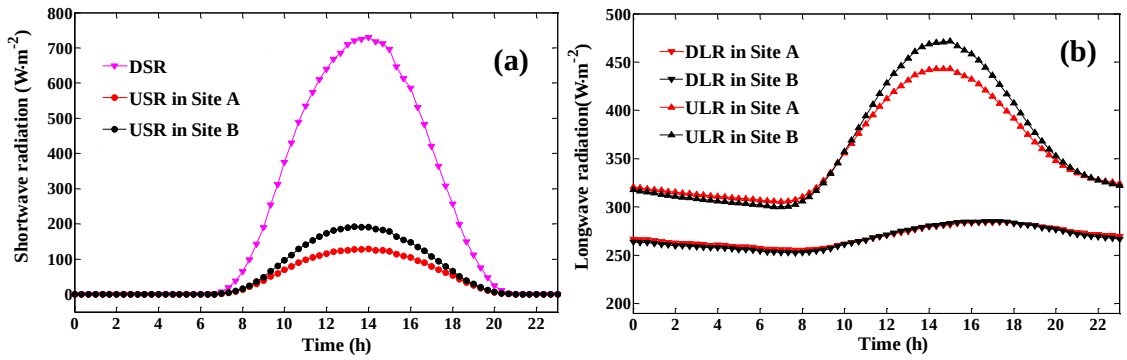

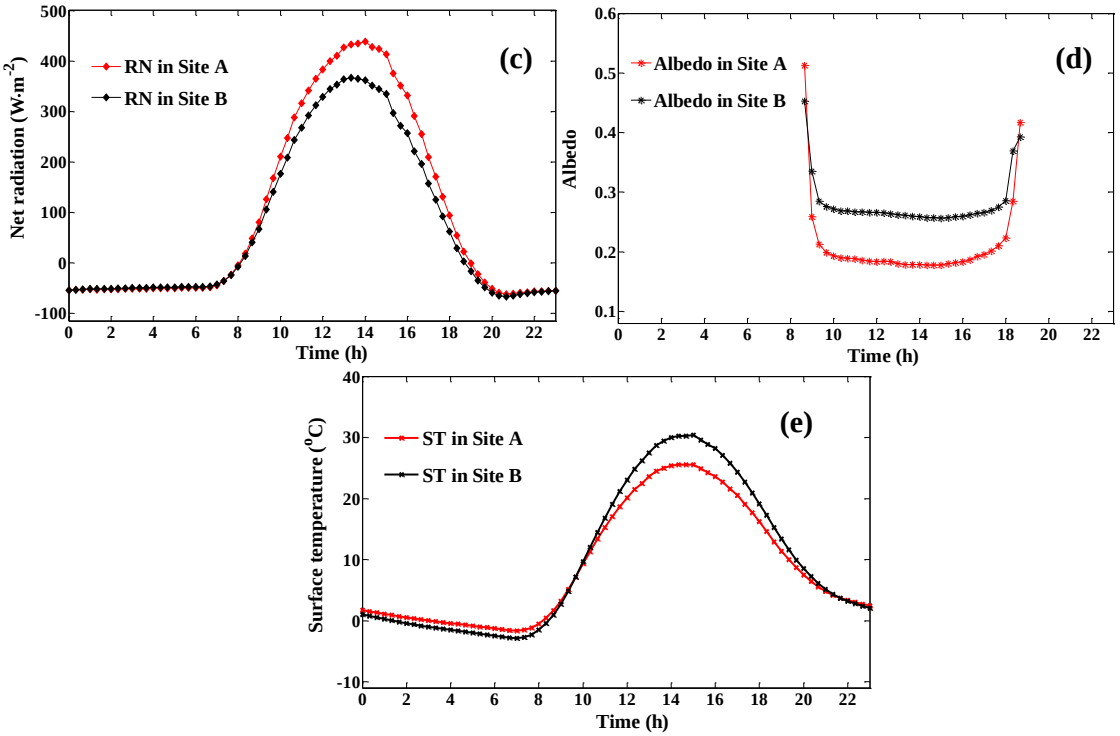

Fig. 3: Annual averaged diurnal variations of radiation components: (a) shortwave radiation, (b) longwave radiation, (c) net radiation, (d) albedo; and (e) surface temperature in the solar farm (Site A) and in the region without PV (Site B) in Golmud.

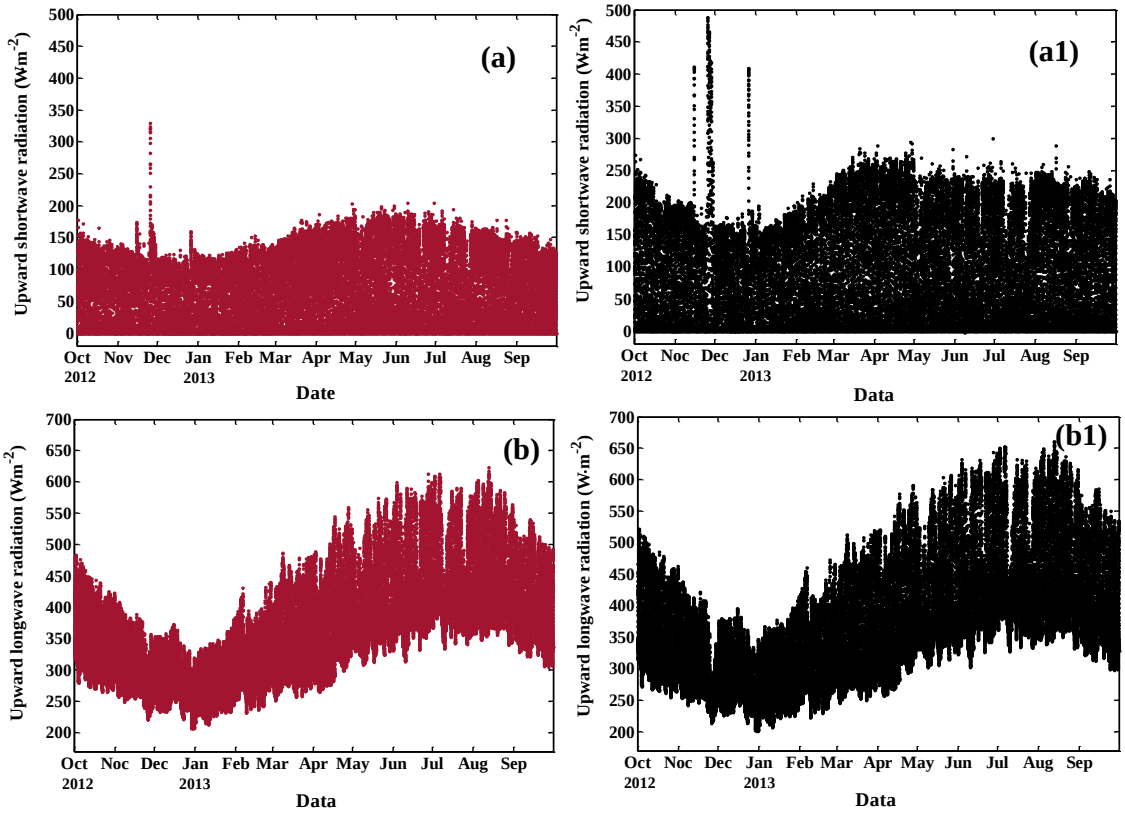

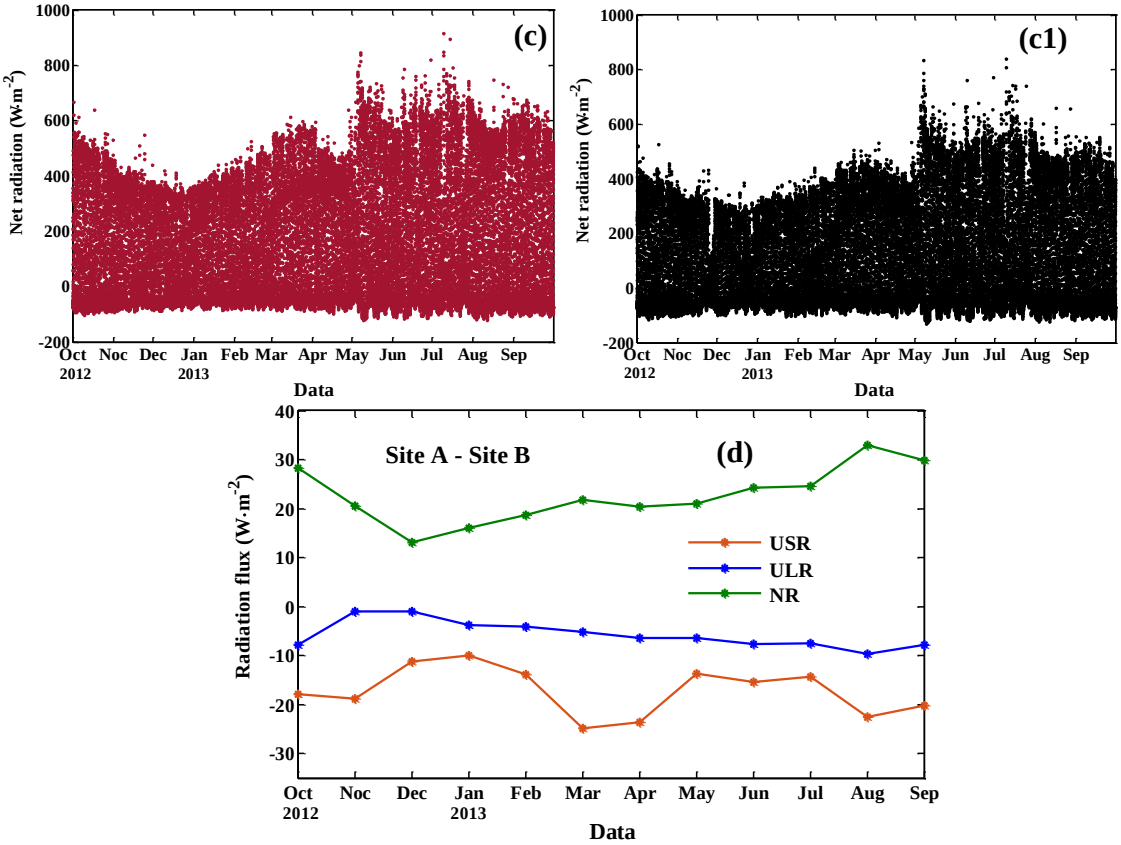

Fig. 4: Annual variation of radiation flux in the solar farm (Site A) and in the region without PV (Site B) in Golmud, where (a), (b) and (c) are the annual variations of USR, ULR and NR in Site A, respectively; (a1), (b1) and (c1) are the annual variations of USR, ULR and NR in Site B, respectively; (d) is the difference of monthly averaged radiation flux between the two sites.

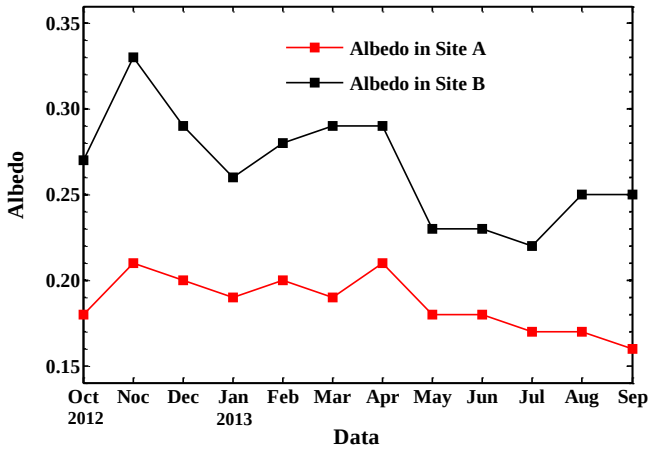

Fig. 5: Annual variation in the monthly averaged albedo in the solar farm (Site A) and in the region without PV (Site B) in Golmud

Tab.2 : Annual mean of the radiation components in the solar farm (Site A) and in the region without PV (Site B) in Golmud

	DSR (W m^{-2})	USR (W m^{-2})	DLR (W m^{-2})	ULR (W m^{-2})	NR (W m^{-2})
Site A	221.83	40.97	269.13	356.17	93.81
Site B	223.37	58.15	267.81	361.87	71.16
Relative difference/%	0.69	29.54	0.49	1.58	31.83

3.2. Comparison of the soil temperatures at the two sites

Soil temperature is one of the most important physical properties in determining the rates and directions of physical

processes of the soil, including energy and mass exchange, evaporation and aeration (Gulser and Ekberli, 2004). However, very few studies have focused on the relationship between the soil temperature and a PV farm. In the present study, the soil temperature data obtained continuously at different depths and at different times of the day from the two sites, from October 2012 to September 2013, were analyzed to reveal the effects of PV arrays on soil temperature in Golmud.

Figure 6 shows the amplitude of the monthly averaged diurnal variation of the soil temperature at the two sites. It shows that the amplitude of the diurnal variation of the soil temperature at the two sites gradually decrease with an increase in soil depth. Moreover, the diurnal variation of the soil temperature at a depth of 5 cm is larger, while the change in the diurnal variation of the soil temperature below the depth of 80 cm does not exceed 0.3℃. The diurnal variation in temperature of each layer of soil between 5 and 40 cm in winter is significantly lower than that in spring, summer and autumn. The maximum value of the amplitude of diurnal variation at a depth of 5 cm at the two sites appeared in August, at 20.8℃ at site A, and at 31.7℃ at site B. The minimum value at site A appeared in January, at 4.6℃, while the minimum value at site B appeared in December, at 18.9℃.

The amplitude of the monthly averaged diurnal variation of the soil temperature at site A is significantly lower than that at site B in the shallow soil layer (5, 10 cm), which is mainly due to the existence of a large number of photovoltaic arrays in the solar farm, making it difficult for the solar radiation to spread in the soil during the daytime, with the soil heat not being able to spread outward easily during the night, resulting in a reduction of the diurnal variation of soil temperature in the solar farm. The thermal insulation effect of the photovoltaic array is particularly evident in the shallow layer of soil.

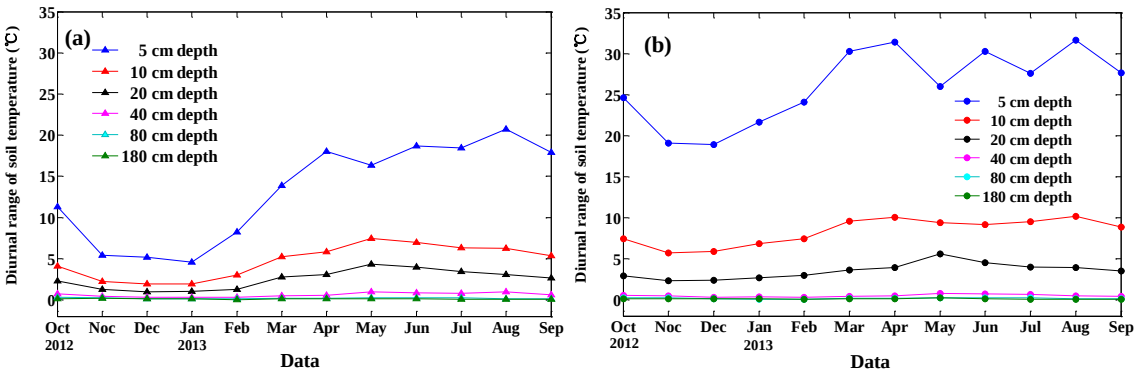

Fig. 6: The amplitude of the monthly averaged diurnal variation of the soil temperature: (a) in the solar farm (Site A) and (b) in the region without PV (Site B).

Figure 7 shows the annual variations of soil temperature at the two sites. As shown in Fig. 7, the changing trend of the annual variations at the two sites is accordant, showing waveform changes. The maximum average soil temperature values at depths of 5–80 cm at the two sites appear in August, while the minimum value appears in January. The maximum average soil temperature values at a depth of 180 cm at the two sites appears in September, while the minimum value appears in February. The average annual soil temperature values at depths of 5–180 cm at site A are 7.5, 7.5, 7.4, 7.6, 7.7, and 7.8℃, respectively, while those at site B are 9.5, 9.4, 9.5, 9.3, 9.4, and 8.9℃, respectively. In winter (December–February), the shadow area of the solar panels reached the maximum, falling onto the site where the soil temperature probes were buried, thus significantly reducing the soil temperature in the solar farm. In winter, the average soil temperature values at depths of 5–180 cm at site A were -10.8, -9.7, -9.1, -7.8, -5.0, and 0.2℃, respectively, while those at site B were -6.2, -5.4, -4.7, -3.2, -0.7, and 3.7℃, respectively. The soil temperatures at different depths in winter in the PV farm were evidently lower than those without PV. Hence, it can be said that the PV farm is a cooling system.

The annual range (annual variation amplitude) of soil temperature at a depth of 5 cm was the largest, with the annual range of soil temperature decreasing gradually, depending on the depth. The annual ranges of soil temperatures at depths of 5–180 cm at site A were 40.4, 37.8, 35.9, 33.4, 27.7, and 19.3℃, respectively, while those at site B were 35.3, 33.2, 31.8, 27.4, 22.1, and 13.6℃, respectively. The annual ranges of soil temperatures at different depths in the solar farm are higher than those in the region without PV.

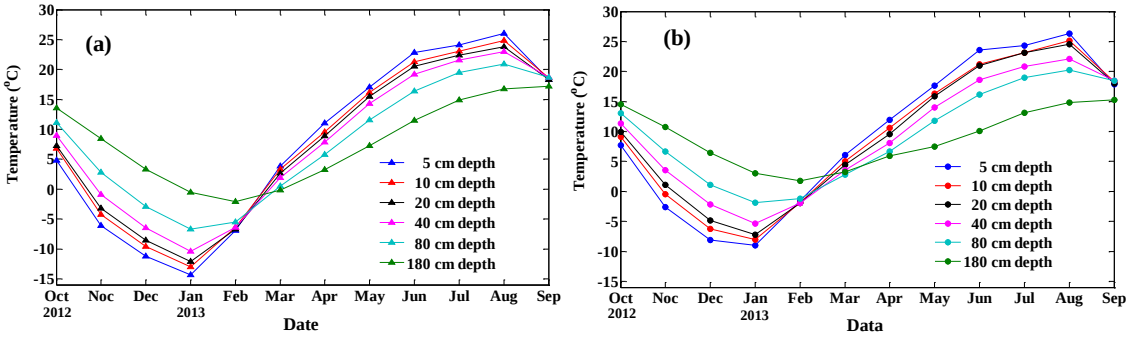

Fig. 7: Seasonal variations in soil temperature: (a) in the solar farm (Site A) and (b) in the region without PV (Site B) in Golmud.

In the PV farm, the presence of the photovoltaic array will affect the solar radiation received on the ground surface, as well as the heat radiating to the atmosphere, thus affecting the soil temperature. A T test was carried out for the daily mean soil temperature at the same depth at the two sites from October 2012 to September 2013 to analyze the influence of the PV array on soil temperature over a year. As shown in Table 3, the data are the P (Probability) values for the T Test (Huang, 1990) at the same depth at the two sites. There are significant differences in the soil temperature at different depths at the two sites from October to March of the following year at the level of 0.05. In addition, there are significant differences at a depth of 80 cm in April and July and at depths of 20 80 cm in August.

The difference between site A and site B at the different depths (the average daily soil temperature at site A, minus the average daily soil temperature at site B) is shown in Fig. 8, hereinafter referred to as the difference. As shown in Fig. 8, the difference in value at the different depths at the two sites from October to March of the following year is mostly below 0℃. Therefore, the average daily soil temperature value in the solar farm is smaller. The average difference in the values at depths of 5 80 cm from October to March of the following year were -3.7, -3.4, -3.7, -3.7, and -3.5℃, respectively.

There is a notable feature, which can be seen in Fig. 8. The difference is very less between the two sites in summer. The possible reason is that the instability of atmospheric stratification of the surface layer and the surface turbulence is strong during summer daytime, resulting in a small temperature difference between the two sites. At the same time, the photovoltaic panels generate heat when they generate electricity during the day, causing the photovoltaic cell panels to have a heating effect on the air temperature of the surface layer, which is stronger in the summer than in the winter. It can also result in a smaller difference of soil temperature between the two sites.

Tab. 3 : The P values for the *T* –Test of the same depth of the two sites

	month											
Depth (cm)	**2012/ 10**	**11**	**12**	**2013/ 1**	**2**	**3**	**4**	**5**	**6**	**7**	**8**	**9**
5	0.018	0.000	0.000	0.000	0.000	0.002	0.393	0.564	0.464	0.901	0.665	0.575
10	0.021	0.000	0.000	0.000	0.000	0.004	0.239	0.825	0.898	0.998	0.433	0.570
20	0.005	0.000	0.000	0.000	0.000	0.002	0.375	0.590	0.418	0.191	0.016	0.593
40	0.005	0.000	0.000	0.000	0.000	0.003	0.707	0.600	0.116	0.070	0.000	0.594
80	0.003	0.000	0.000	0.000	0.000	0.000	0.025	0.568	0.495	0.001	0.000	0.425

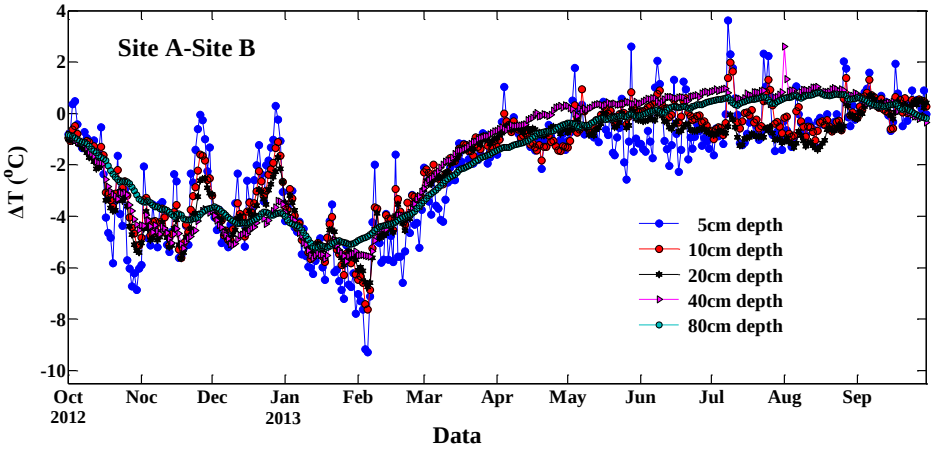

Fig. 8: Annual variations of difference value of different layers of soil temperature between the two sites

Figure 9 shows the annual variations of thermal conductivity at 5–20 cm depths at the two sites. Thermal conductivity in the soil may be explained as the quantity of heat flow through an area of soil per unit time and temperature gradient. The existing research shows that soil thermal conductivity is mainly influenced by soil texture and moisture content (Peterslidard et al., 1998). The soil texture of the two sites is the same; thus, thermal conductivity is mainly affected by the soil moisture content.

As shown in Fig. 9, the monthly mean thermal conductivity reached a maximum in May and a minimum in September at the two sites. Each monthly mean thermal conductivity at the PV farm is higher than that in the region without PV, with the difference being evident. The main reason could be the higher soil moisture in the solar farm. The photovoltaic panels increase the roughness, playing an important role in weakening the wind velocity. At the same time, solar radiation received by the surface in the solar farm is less than that in the region without PV. These factors decrease the evaporation of soil in the solar farm, thus increasing the soil moisture.

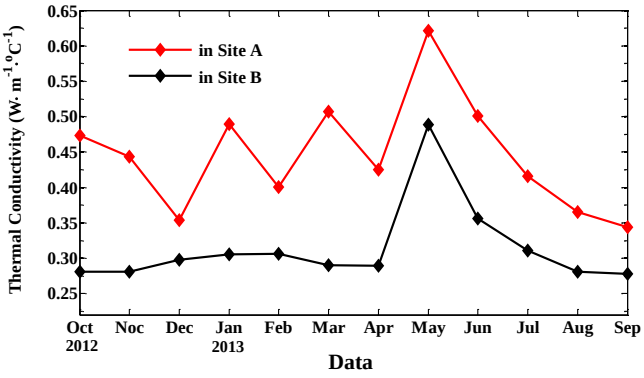

Fig. 9: Annual variation in the monthly mean thermal conductivity in the solar farm (Site A) and in the region without PV (Site B) in Golmud

3.3. Comparison of air temperatures at the two sites

The observational data we used are from May 2013 to April 2014. Figure 10 shows the diurnal variations of the 2-m air temperature and the differences (site A to site B) during the four seasons. July, October, January and April were selected to represent the four seasons of the year. The results show that the air temperature at a height of 2 m at the two sites is essentially the same during winter daytime, but in the other seasons, the daytime air temperature at the PV farm is higher than that in the region without PV. The maximum difference appears during the summer daytime, with a value of 0.7℃ (the summer daytime averaged value). This is because the solar panels enhance the local atmospheric turbulence flow and the heat transfer, as well as radiate heat during the day. Moreover, its effect of heating the air is greater during summer, when the irradiance is higher. As Fthenakis et al. (2013) observed, the PV module temperatures were consistently higher than those of the surrounding air during the day. The nighttime air temperature at a height of 2 m during the four seasons at the solar farm was higher than that in the region without PV arrays, since the solar panels have a heat preservation effect near the ground. The differences in values between the two sites were 0.1, 0.3, 0.2, and 0.1℃ in summer, autumn, winter and spring, respectively.

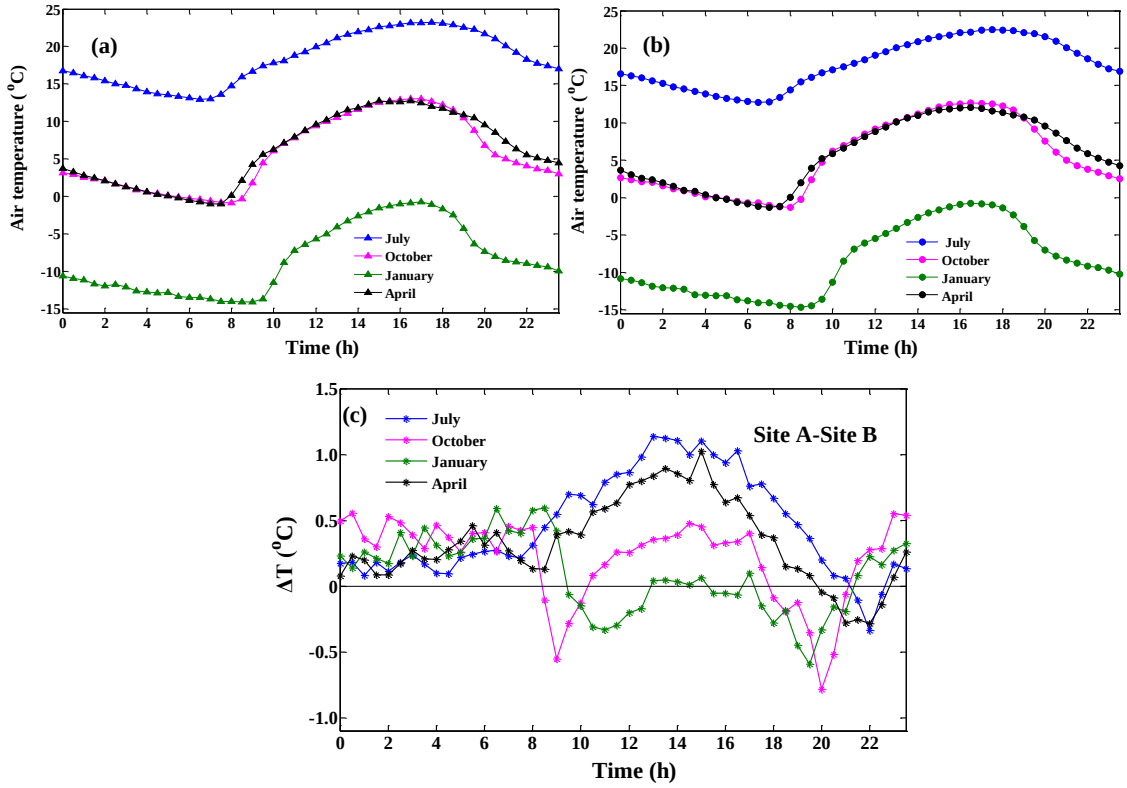

Fig. 10: Diurnal variations of 2 m- air temperature in the four seasons: (a) in the solar farm (Site A), (b) in the region without PV (Site B) and (c) difference between the two sites.

4. Conclusion

Based on the field observation data from the large solar farm and the region without a PV array in Golmud, the characteristics of surface radiation were analyzed. The results show that the total daily values of upward shortwave radiation and net radiation at the two sites are significantly different. The mean daily albedo at the solar farm is 0.19, while it is 0.26 in the region without PV. The annual mean of net radiation at the solar farm is evidently higher than in the region without PV, indicating that the solar farm is collecting energy. However, the PV array converts a part of the radiation energy to electrical energy for output, which can cause the surface layer temperature at the solar farm to be lower.

The characteristics of soil temperature were also analyzed. The results show that the daily range of soil temperature at a depth of 5–10 cm at the solar farm is lower than that in the region without PV farm. Therefore, the solar photovoltaic arrays demonstrated thermal insulation performance. The annual range of soil temperature at a depth of 5–180 cm at the solar farm was larger than that in the region without PV. The soil temperature at different depths during winter at the solar farm was clearly lower than that in the region without PV, indicating that the PV farm is a cooling system. The daily mean of the soil temperature at a depth of 5–80 cm from October 2012 to March 2013 was evidently lower than that in the region without PV array.

The characteristics of diurnal and annual variation features of the 2-m air temperature were analyzed at the two sites. The results show that the air temperature at a height of 2 m at the two sites is essentially the same during winter daytime, while during the other seasons, the daytime air temperature at the PV farm is higher than that in the region without PV. The maximum difference appears during the summer daytime, as the solar panels radiate heat during the daytime. This effect of heating the air is greater in summer. The nighttime air temperature at a height of 2 m during the four seasons at the solar farm is higher than that in the region without PV arrays, since the solar panels exhibit heat preservation effect near the ground.

5. References

Fthenakis, V., Yu, Y., 2013. Analysis of the potential for a heat island effect in large solar farms. IEEE, Photovoltaic Specialists Conference. 2, 3362-3366.

Gagnon, L., Belanger, C., Uchiyama, Y., 2002. Life-cycle assessment of electricity generation options: the status of research in year 2001. Energy Policy. 30, 1267-1278.

Gao, Z., Wang, L., Horton, R., 2009. Comparison of six algorithms to determine the soil thermal diffusivity at a site in the loess plateau of China. Hydrol. Earth Syst. Sci. Discuss. 6, 51-60.

Genchi, Y., Sugawara, Y., Ohtomo, J., Wen, C., Takahashi, H., Inaba, A., 2002. Development of a heat balance model of photovoltaic cells to assess PV installation impacts on the urban heat island effect. Environ. Syst. Res. 30, 271-276.

Gulser, C., Ekberli, I., 2004. A comparison of estimated and measured diurnal soil temperature through a clay soil depth. J. Appl. Sci. 4, 418-423.

Horton, R., Wierenga, P. J., Nielsen, D. R., 1983. Evaluation of methods for determining the apparent thermal diffusivity of soil near the surface. Soil Sci. Soc. Am. J. 47, 25-32.

Huang, J., 1990. Meteorological statistical analysis and forecast method. Beijing: China Meteorological Press. 18-27.

Kämpf, J. H., Montavon, M., Bunyesc, J., Bolliger, R., Robinson, D., 2010. Optimisation of buildings' solar irradiation availability. Sol. Energy. 84, 596-603.

Li, S., Lü, S., Ao, Y., Shang, L., 2009. Annual variations in the surface radiation budget and soil water and heat content in the upper yellow river area. Environ. Geol. 57, 389-395.

Liu, X., Hoekman, S.K., Robbins, C., Ross, P., 2015. Lifecycle climate impacts and economic performance of commercial-scale solar PV systems: A study of PV systems at Nevada's Desert Research Institute (DRI). Sol. Energy. 119, 561-572.

Matzinger, N., Andretta, M., Gorsel, E. V., Vogt, R., Ohmura, A., Rotach, M. W., 2002. Surface radiation budget in an alpine valley. Q. J. Roy. Meteor. Soc. 129, 877-895.

Nemet, G.F., 2009. Net radiative forcing from widespread deployment of photovoltaics. Environ. Sci. Technol. 43, 2173-2178.

Pessacg, N.L., Solman, S. A., Samuelsson, P., Sanchez, E., Marengo, J., Li, L., et al., 2013. The surface radiation budget over South America in a set of regional climate models from the Claris-Lpb project. Clim. Dyn. 43, 1221-1239.

Peterslidard, C.D, Blackburn, E., Liang, X., Wood, E.F., 1998. The Effect of Soil Thermal Conductivity Parameterization on Surface Energy Fluxes and Temperatures. J. Atmos. Sci. 55, 1209-1224.

Taha, H., 2013. The potential for air-temperature impact from large-scale deployment of solar photovoltaic arrays in urban areas. Sol. Energy. 91, 358-367.

Tian, W., Wang, Y., Xie, Y., Wu, D., Zhu, L., Ren, J., 2007. Effect of building integrated photovoltaics on microclimate of urban canopy layer. Build. Environ. 42, 1891-1901.

Turney, D., Fthenakis, V., 2011. Environmental impacts from the installation and operation of large-scale solar power plants. Renew. Sustain. Energy Rev. 15, 3261-3270.

Tyagi, B., Satyanarayana, A. N. V., Kumar, M., Mahanti, N. C., 2012. Surface energy and radiation budget over a tropical station: an observational study. Asia.-Pacific. J. Atmos. Sci. 48, 411-421.

Wang, K., Liang, S., 2009. Evaluation of aster and modis land surface temperature and emissivity products using long-term surface longwave radiation observations at surfrad sites. Remote Sens. Environ. 113, 1556-1565.

Zhang, L., Zhang, L., Wang, Y., 2016. Shape optimization of free-form buildings based on solar radiation gain and space efficiency using a multi-objective genetic algorithm in the severe cold zones of China. Sol. Energy. 132, 38-50.